Engineering Failure Analysis 127 (2021) 105562

Contents lists available at ScienceDirect

Engineering Failure Analysis

journal homepage: www.elsevier.com/locate/engfailanal

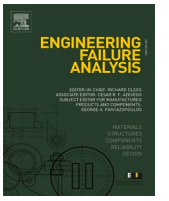

Chloride stress corrosion cracking of a non-standard, 'Borderline' Chromium-Manganese stainless steel – Problems of counterfeits and substandard materials

K.H. Chu [a,1], C.C. Lam [a,1], Y.F. Sun [b], V.A.M. Cristino [a], C.T. Kwok [a,c], H. Pan [c,d], K. H. Lo [a,c,*]

[a] Department of Electromechanical Engineering, Faculty of Science and Technology, University of Macau, Macau SAR, China
[b] School of Materials Science and Engineering, Zhengzhou University, Zhengzhou, China
[c] Institute of Applied Physics and Materials Engineering, University of Macau, Macau SAR, China
[d] Department of Physics and Chemistry, Faculty of Science and Technology, University of Macau, Macau SAR, China

ARTICLE INFO

Keywords:
Chromium-manganese stainless steel
Chloride stress corrosion cracking
Slow strain rate test
Counterfeit

ABSTRACT

Nonstandard chromium-manganese (stainless) steels are gaining popularity nowadays, but data for them are inadequate as the majority of literature is on the 'pedigrees' such as the standard 200 series and 300 series steels. This paper begins with a brief overview of the counterfeit problems of such steels. It then presents the slow-strain-rate test results of a chromium-manganese 'borderline' stainless steel in room-temperature air, 60 °C NaCl and 60 °C distilled water (the lower-bound temperature for chloride stress corrosion cracking in austenitic stainless steels). At low strain rates (10^{-6} s^{-1}), grain-boundary segregation of phosphorus and sulphur (especially the latter) can cause intergranular cracking in air and in 60 °C distilled water. In 60 °C NaCl, manganese sulphides may serve as the initiation sites of transgranular cracking. Many producers of nonstandard chromium-manganese (stainless) steels lack impurity control technologies, and so users must be vigilant of this issue. The fracture mode of the 'borderline' stainless steel is strain-rate dependent, changing from being mainly intergranular to being transgranular and dimpled as the strain rate goes up. The reason behind this is unclear, but a plausible suggestion is given in this paper.

1. Counterfeiting and the lean austenitic stainless steels

Failures caused (partly or entirely) by the use of substandard materials are not rare [1–4]. A material may become substandard because of poor workmanship, improper manufacturing/heat-treating processes [2,4,5], and non-conformance of composition to standards [3].

Stainless steels derive their excellent corrosion resistance from pricey alloying elements such as chromium, nickel, and molybdenum. For a particular grade of stainless steels, its substandard counterparts typically have less of these expensive alloying elements. On the other hand, elements such as phosphorus, oxygen and sulphur may be higher than expected, especially for the steels made by smaller, older mills [6]. Premature failures may occur because of this composition issue [7–9].

* Corresponding author.
E-mail address: fstkhl@um.edu.mo (K.H. Lo).
[1] Equal First Authors.

https://doi.org/10.1016/j.engfailanal.2021.105562
Received 31 March 2021; Received in revised form 1 June 2021; Accepted 21 June 2021
Available online 23 June 2021

The 300 series austenitic stainless (chromium-nickel) steels are used extensively in a wide variety of applications. Because of health concern and cost factor, nickel has been replaced (partially or completely [10]) by manganese and nitrogen, resulting in the lean grades. These are usually designated as the 200 series austenitic stainless steels [11–13]. According to the International Stainless Steel Forum, the lean 200 series steels are sometimes mis-classified as their more expensive 300 counterparts [11]. As a matter of fact, cases involving bogus 300 series steels (whose compositions are similar to that of the borderline steel used in this paper) have been reported recently [3,14].

In one case, the bolts used in the pressure gauges of a gas fuel system were found to be made of a chromium-manganese austenitic steel, but they were falsely claimed to be made of the ASTM 316 austenitic stainless steel [3]. A similar incidence was also reported for the threaded joint of a reabsorption tower [14]. From these examples and the press release by the European Anti-Fraud Office [15], it may be seen that the problems of counterfeits and substandard metals are becoming increasingly widespread.

It must be pointed out that the chromium-manganese 'borderline' stainless steel of this paper (called 'the present steel' hereinafter) might not necessarily be a counterfeit. As a matter of fact, many chromium-manganese steels are not covered by international specifications and codes [6,11,13], and are only identified by their producer-specific brand names [11]. These steels are sold explicitly as cheap alternatives to their more expensive pedigree counterparts such as the 300 series steels.

The rationale of this paper is as follows: The cases involving the bogus 300 series steels just mentioned, and the increasingly widespread use of the non-standard chromium-manganese (stainless) steels clearly show the necessity of providing more data to the users of these kinds of steels. Note that the users may unwittingly use these steels as they are deceived by unscrupulous suppliers, or the users may be fully aware of the fact that these are inadequate steels and intentionally use them for less demanding applications. Irrespective of the reason, data for these steels are currently rather lacking. For example, a search of the literature of austenitic stainless steels will show that the majority of papers are on the pedigree types of steels, and so even the intentional users of nonstandard steels will have no guides to rely on. Since similar nonstandard manganese-containing borderline stainless steels have been developed for different applications [16], it should be useful to undertake research on them so as to provide more data to their users. Such data may also facilitate failure analysis of components/structures made of these nonstandard steels.

2. Materials and experimental details

The composition of the present steel, as measured by spark optical emission spectroscopy, is shown in Table 1. The main alloying elements are chromium and manganese, with some nickel. The samples were solution-treated at 1100 °C for 1 h, and then rapidly quenched into water.

Slow-strain-rate tensile tests (SSRT tests) were conducted in air (about 25 ℃), in distilled water (60 ℃) and in 3.5% NaCl (60 ℃) at a strain rate of 10^{-6} s^{-1} by using an SSRT tester (Model SCC-SSRT-50, Advance Instrument Inc). Multiple SSRT tests were done for each testing medium. Two SSRT curves representing the envelope of the results are reported for each of the testing medium. The choice of 60 ℃ for conducting the SSRT tests is explained in the discussion part. A few tests were done using the AISI 304 austenitic stainless steel for comparison purposes. To avoid cluttering up the figures and since the results obtained from the AISI 304 steel were much more repeatable than those of the chromium-manganese steel, only one SSRT curve representing the general trend is shown for the AISI 304 steel. In order to look into the effects of strain rates on the fracture behaviour of the present steel in air, tensile tests at a strain rate of 10^{-1} s^{-1}were done by using an INSTRON 5567 tensile tester.

A VersaSTAT 3F potentiostat was used for cyclic potentiodynamic polarisation tests. A saturated calomel electrode (SCE) served as the reference electrode and two parallel graphite rods were used as the counter electrodes. The electrolyte used was 3.5% NaCl at 25 °C and the sweep rate was 1 mV/s. For each condition, polarisation tests were repeated five times. The two polarisation curves representing the envelope of the results obtained from the borderline stainless steels are reported.

A Hitachi S-3400 N Type I scanning electron microscope was used to examine the samples after SSRT tests and corrosion experiments. The samples for optical metallography were ground with abrasive papers up to 1000 grit and then polished with diamond paste. Subsequently, they were electrolytically etched with 10% oxalic acid (5 V for about 10 s). X-ray diffraction (XRD) measurements were conducted with a Rigaku MiniFlex 600 X-ray diffractometer (CuKα) at a scan rate of 0.1°/s to identify the phases of the solution-treated samples.

3. Results and discussion

3.1. Alloying elements of the present steel

The present steel was branded by its seller as an economical, lean austenitic stainless steel. Among the standard lean grades, the type 201 steel is arguably the most popular. As shown in Table 1, the present steel has much lower nickel content than the 201 steel.

Table 1
Measured composition of the chromium -manganese 'borderline' stainless steel and the nominal composition of the 201 austenitic stainless steel (wt %).

	Cr	Mn	Ni	Mo	Si	Cu	S	P	C	N
Present Steel	10.11	10.12	1.21	0.04	0.52	0.42	0.08	0.03	0.30	0.09
Standard 201 steel	16.00–18.00	5.50–7.50	3.50–5.50	—	1.00 Max	—	0.030 Max	0.060 Max	0.15 Max	0.25 Max

This is understandable, as the present steel would not have been advertised as an economical one otherwise.

The minimum content of chromium for steels to attain stainlessness is stated to be 10.5% [17]. The chromium content of the present steel slightly falls short of this threshold. However, taking into account the error of the spark-OES measurement, the present steel might be considered a 'borderline' case. The manganese content of the present steel is higher than the 201 steel and it sits within the range typical of medium manganese steels [18].

The present steel has 0.42 wt% copper. For some of the steels in the 200 series, up to 3 wt% of copper is purposefully added for formability [19]. Nevertheless, copper may sometimes be an unintentional element [20]. It is not known whether copper was intentionally added to the present steel or its presence was due to the use of copper-tainted iron scrap raw material.

The carbon content of the present steel is double of the upper limit of 0.15 wt% allowed for the 201 steel. A high carbon content may result in easy sensitisation, which is a common cause of failure in practice [21]. However, because carbon is a good strengthener if it is in solid solution, it is purposefully used in some high-interstitial FeCrMnNiNC-based austenitic stainless steels for strengthening purposes and for increasing the solubility of nitrogen [22]. Nonetheless, the nitrogen content of the present steel is not high at all. Therefore, it is speculated that the high carbon content of the present steel is not for increasing the solubility of nitrogen.

Phosphorus and sulphur are generally considered deleterious, although the former can act as a strengthener [23,24] and the latter may improve machinability [19]. These two elements may segregate to grain boundaries and cause their weakening [25]. Corrosion resistance may also suffer [26]. For manganese-containing steels, the formation of manganese sulphides can be problematic [27]. It should be noted that poor control of trace elements is a well-known problem for the economical stainless steels [6,11,13], as many of them are produced by small mills that lack the technologies of impurity control [6].

3.2. Microstructural characterisation

The microstructure of the present steel in the solution-treated condition is shown in Fig. 1, in which etch pits associated with precipitates may be seen. These precipitates were mostly manganese sulphides (as will be discussed below). In some grains, streaks existed and they were likely to be the epsilon (ε) and the alpha-prime (α') martensites, as shown by XRD and the Klueh constitution diagram below.

The XRD spectrum of the present steel after solution treatment shows that it contained the alpha-prime martensite and the epsilon martensite (Fig. 2). Since the α'(1 1 1) and the ε(0 0 2) peaks are near each other, it's necessary to zoom into the 2θ range of 42° and 46° for a better view of them. However, the two peaks still could not be clearly resolved, as they agglomerated to form a broad peak (inset of Fig. 2). The presence of the two martensites may be understood with reference to the Klueh diagram [28].

The Schaeffler diagram is often used for the prediction of phase constitution of austenitic-steel weld metals, and for guiding the design of new stainless steels [29]. A modified version of the Schaeffler diagram was proposed by Klueh et al [28] for manganese-containing steels, which has been shown to be satisfactory for these steels in the solution-treated condition [30]. According to the Klueh diagram, the present steel is surely not fully austenitic (Fig. 3). In the original Schaeffler diagram, the present steel might possibly fall into the single-phase austenite region (taking into consideration of the errors of element-content measurements). Nevertheless, even if this is the case, the present steel would still be adjacent to the boundaries of the single-phase austenite region. Hence, the phase prediction result given by the Klueh diagram for the present steel corroborates with the XRD spectrum.

3.3. Corrosion tests

The cyclic polarisation curves of the present steel after solution treatment are shown in Fig. 4. For comparison purposes, the polarisation curve of the solution-treated AISI 304 austenitic stainless steel is also shown. The present steel had a shorter passive range

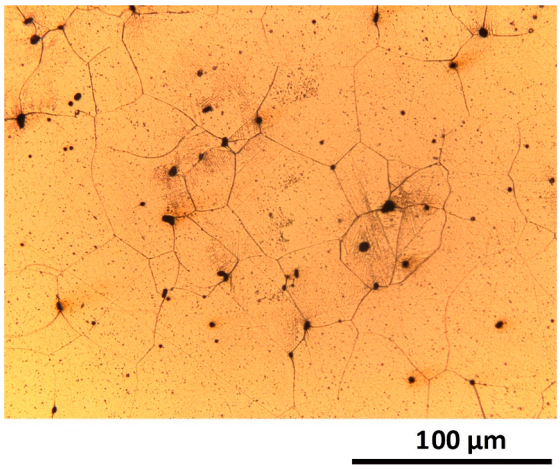

Fig. 1. Microstructure of the present steel after solution treatment.

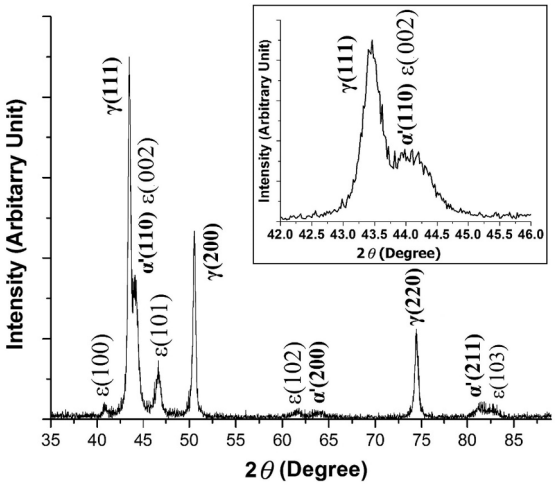

Fig. 2. XRD spectrum of the present steel after solution treatment.

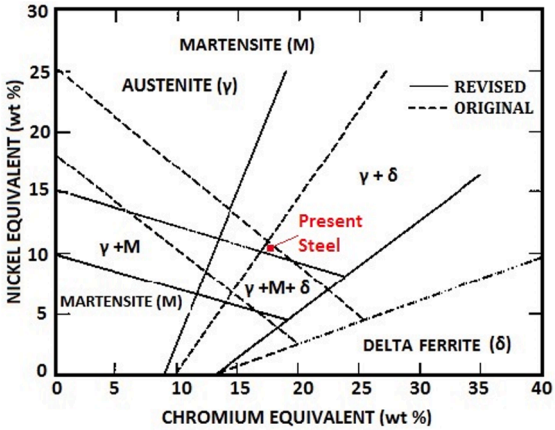

Fig. 3. Phase make-up of the present steel predicted by the Klueh diagram (Reused with permission from Elsevier. The texts were edited for clarity by the present authors) [28]

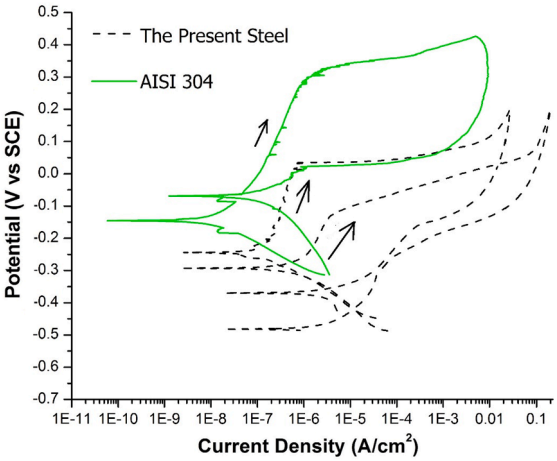

Fig. 4. Cyclic polarisation curves of the present steel and the AISI 304 steel.

and a lower pitting potential relative to the AISI 304 steel. This inferiority of the present steel is due to its lower contents of alloying elements.

In Fig. 4, it may be seen that the difference between the borderline steel and the genuine 304 steel can be quite large (let alone bogus steels whose alloying contents can be much lower than the present borderline steel). Nonstandard steels having compositions similar to that of the present borderline steel have been reported to be passed off as the genuine 300 series steels, causing premature failure [3,14].

Impurity elements such as phosphorus may segregate to grain boundaries and cause intergranular corrosion. For the present steel, however, no grain boundaries had been revealed after cyclic polarisation tests in 3.5% NaCl (Fig. 5). A close-up view of a corrosion pit is also shown in the figure. The pitting corrosion attacks most likely started from inclusions such as manganese sulphides (see discussion below).

To ascertain the nature of the precipitates, the fracture surface of the present steel pulled to failure in air at a much higher strain rate (10^{-1} s^{-1}) was examined. Fig. 6 shows that the fracture surface of the present steel was transgranular and dimpled at this high deformation speed. Also, a number of inclusions residing in some of the dimples can be seen in the figure. From the mappings of the major elements (i.e. iron, chromium, and manganese) and sulphur, it can be seen that most of the inclusions were particularly enriched with manganese and sulphur. Therefore, most of the inclusions were likely to be manganese sulphides. The distribution of chromium was relatively uniform, and so there were no (or nearly no) chromium-rich carbides in the present steel after solution treatment.

3.4. Slow-Strain-Rate tests

SSRT tests were done in air (about 25 ℃), in distilled water (60 ℃) and in 3.5% NaCl (60 ℃). The testing temperature of 60 ℃ was chosen for the following reasons: Firstly, Yoon et al [31] developed some medium manganese stainless steels and studied their chloride stress corrosion cracking (Cl-SCC) behaviour. According to these authors (who used 50 °C), most of the literature dealing with the Cl-SCC of austenitic stainless steels used boiling $MgCl_2$, whereas aqueous NaCl at lower temperatures would be more relevant to the service conditions. Some practical examples of stainless steel components working around 60 °C are the heat exchanger plates of the residential heating systems [32] and brine recirculation pumps [33]. Secondly, some producers do explicitly advertise similar chromium-manganese borderline steels as economical alternatives to the genuine 200 or 300 series steels for less demanding applications. In this case, the users will be completely in the know about the lower quality of their steels and so will not use them in the harsh environments designed for their 200 or 300 series counterparts. Since the chromium content of the present steel borders the commonly accepted threshold of 10.5 wt% [17], and since many researchers and analysts of corrosion failures view 60 ℃ as the lower-bound temperature for the occurrence of Cl-SCC in austenitic stainless steels [34–36], it was decided to perform SSRT tests at this temperature.

The in-air SSRT curves of the present steel and the AISI 304 steel in the solution-treated condition are shown in Fig. 7. The present steel had a much lower ductility than the AISI 304 steel. However, its strain-hardening capability and strengths were higher. The higher strain-hardening capability of the present steel is due to the presence of manganese [37,38], while the higher strength could be due to its high carbon content.

3.4.1. Effects of testing media

The SSRT curves of the different samples are shown in Fig. 8. This figure shows that replacing air with 60 °C distilled water caused a small softening. The average ductility, however, was not much affected. The SSRT curves obtained with 60 °C NaCl did not show much change of average ductility. However, the average ultimate tensile strength turned out to be higher than in 60 °C distilled water by a very small margin. These SSRT results were not anticipated, and their discussion will be presented after examining the side surfaces of the SSRT samples. It should be pointed out that from Figs. 4 and 8, it may be seen that the corrosion and SSRT results obtained from the present borderline steel had noticeable variability, which could be caused by compositional inhomogeneity and lack of composition

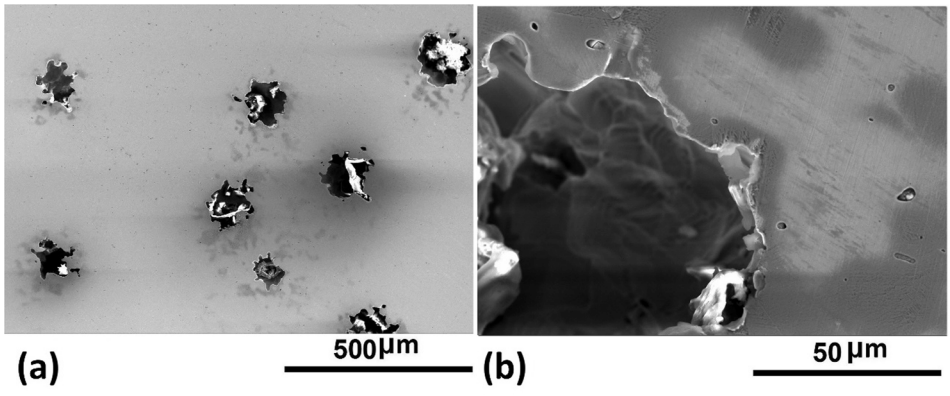

Fig. 5. (a) Surface appearance of the present steel after cyclic polarisation tests, and (b) close-up of a pit.

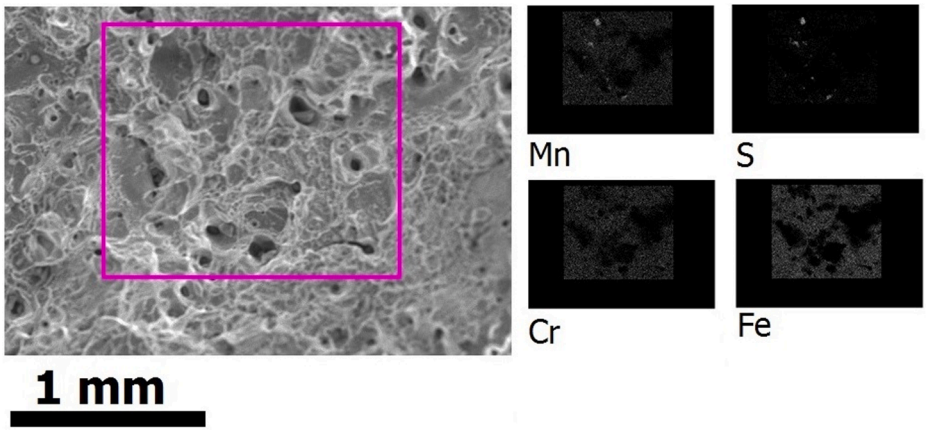

Fig. 6. Selected elemental mappings obtained from the fracture surface of a sample pulled to failure in air at a strain rate of 10^{-1} s^{-1}.

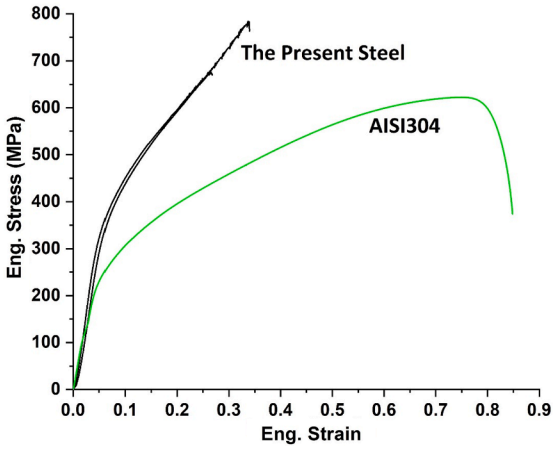

Fig. 7. SSRT curves (in air) of the present steel and the AISI 304 steel.

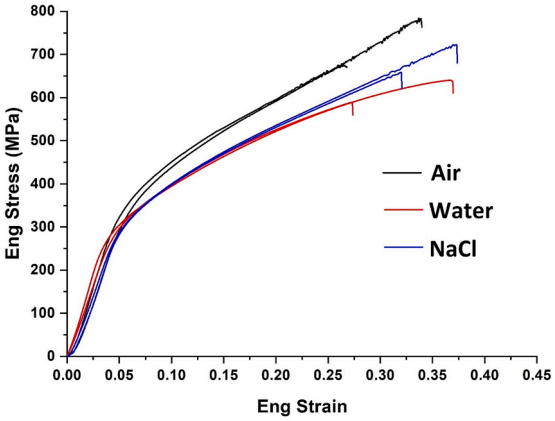

Fig. 8. SSRT curves of the present steel in different media.

control, as stated in Section 3.1.

It was originally thought that the present steel would not be corroded too much in 60 °C distilled water. However, it turned out that it did suffer from corrosion (Fig. 9). As shown in the figure, even though the present steel was in the solution-treated state, corrosion had occurred and numerous short cracks had formed on the samples during SSRT tests in both 60 °C distilled water and NaCl. These

short cracks are indicative of SCC [22,39].

The side cracks on the samples SSRTed in water tended to be less numerous and longer than those on the samples SSRTed in NaCl (Fig. 9, and Fig. 10. (a) and (c)). When these side cracks were examined at a higher magnification, it can be seen that the surface fracture of the samples SSRTed in distilled water was predominantly intergranular (Fig. 10 (b)). When the present steel was SSRTed in air, the fracture surface was also mostly intergranular (Fig. 11(a)). However, the surface fracture of the samples SSRTed in 60 °C NaCl was mostly transgranular (Fig. 10 (d)).

Fig. 9 shows that even in the solution-treated condition and being tested in air, the present steel did not show necking, but its ductility was not low. Note that the present steel did have about 10 wt% of chromium and a small amount of nickel. Therefore, the short cracks and corrosion of the samples SSRTed in 60 °C distilled water lay bare the danger of using the present steel in even mildly corrosive environments. The short cracks and corrosion were most likely caused by the segregation of impurity elements to grain boundaries. For similar economical chromium-manganese steels, the control of impurity contents such as phosphorus and sulphur is therefore critical.

For the present steel, Fig. 9 shows that the sample SSRTed in 60 °C NaCl had sustained heavier corrosion attacks. The harmful effects of chlorine (which were imposed to the present steel on top of the effects of impurities), however, were not particularly obvious. The average strength of the samples SSRTed in NaCl actually was higher than that of the samples SSRTed in distilled water by a small margin. The reason is unknown at the moment, but it could be due to the intergranular cracking mode.

One more point to note of Fig. 8 is that the present steel had a slightly better strain-hardening capability in 60 °C NaCl than in 60 °C distilled water. It is the belief of some researchers that intergranular cracking implies a higher susceptibility to SCC than transgranular cracking [40]. It was found that adding molybdenum (up to 1.760 wt%) to an FeCrMnNiCN austenitic stainless steel could reduce its susceptibility to Cl-SCC and the extent of intergranular fracture [22]. The intergranular cracking associated with grain-boundary segregation of phosphorus and sulphur in 60 °C distilled water caused a gradual decrease of strain-hardening rate of the present steel. In 60 °C NaCl, the cracking mode became transgranular with in-grain manganese sulphides being some of the possible crack initiation sites. The strain-hardening rate remained more or less constant without any gradual decrease.

To sum up, it may be seen that for the present 'borderline' chromium-manganese stainless steel, its tensile behaviour was not too bad in air. Nevertheless, even if the environment was just mildly corrosive, the present steel still suffered from corrosion because of its high levels of impurities (in spite of the fact that it contained about 10 wt% chromium). Short cracks suggestive of SCC may be seen on the samples SSRTed in 60 °C distilled water. However, ductility was not much reduced, and strength was just compromised to a small extent. In 60 °C NaCl, the present steel suffered from heavier corrosion attacks. Its SSRT behaviour, however, did not worsen too much relative to that in 60 °C distilled water. The similarity in SSRT behaviour of the present 'borderline' stainless steel, which contains relatively high levels of impurity, in both distilled water and NaCl means cautions must be exercised even when it is used in relatively benign aqueous environments. The same cautions could be applicable to other similar economical steels and counterfeits (much lower alloying contents and even looser impurity control are expected for the latter).

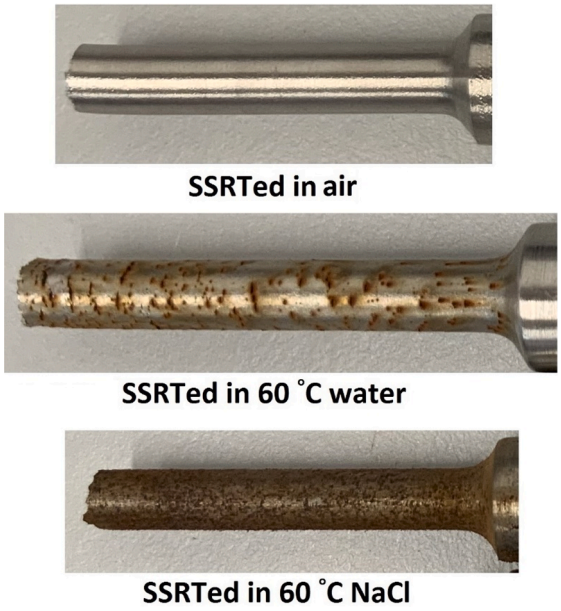

Fig. 9. Photographs showing the samples SSRTed in different media.

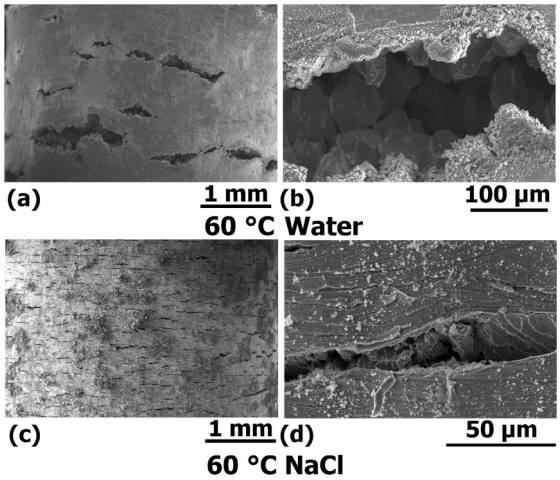

Fig. 10. Cracks on the side surfaces of samples SSRTed in 60 °C distilled water ((a) and (b)), and in 60 °C NaCl ((c) and (d)).

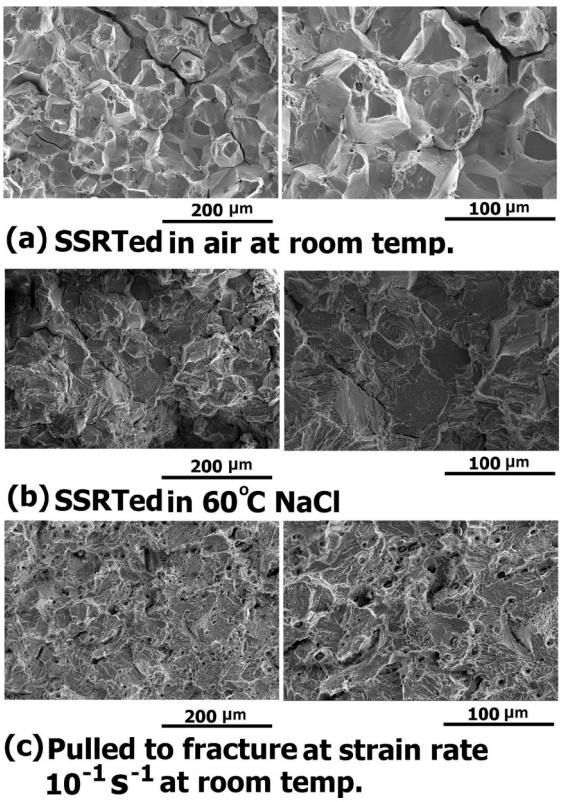

Fig. 11. Fracture surfaces of the present steel after being (a) SSRTed in air, (b) SSRTed in 60 °C NaCl, and (c) pulled to failure in air at a strain rate of 10^{-1} $s^{-1.}$

4. Fractography

4.1. Fracture surface analyses of SSRT test samples

When the present steel was SSRTed in air and in 60 °C distilled water, its fracture surface showed predominantly intergranular cracking mode (Fig. 10(b) and Fig. 11(a)). However, some grains were cleaved through transgranularly (see the lower left part of Fig. 11(a) and Fig. 12). In Fig. 12, a transgranular crack is clearly shown. When the present steel was SSRTed in 60 °C NaCl, the

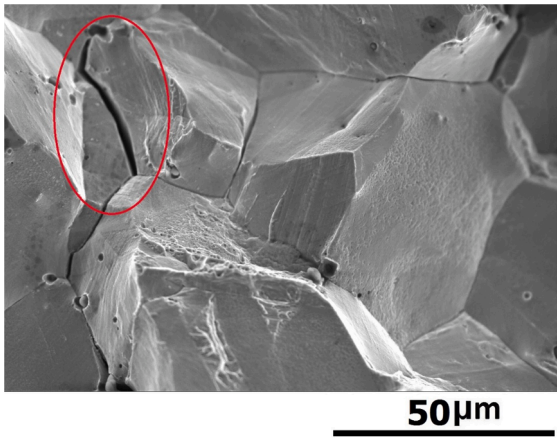

Fig. 12. High-magnification view showing a transgranular crack (within the loop) of a sample SSRTed in air.

cracking mode was predominantly transgranular (Fig. 10(d) and Fig. 11(b)).

For the present steel, the intergranular cracking mode in air and in 60 °C distilled water should be due to its high phosphorus and sulphur contents. Phosphorus may reduce the intergranular corrosion resistance of austenitic stainless steels [41] and weaken grain boundaries of austenitic steels [42]. Sulphur is also known to aid intercrystalline cracking [43]. From Fig. 10 (a) and (b), it may be seen that the surface cracks initiated at and then grew along grain boundaries.

The phosphorus content of the present steel was 0.03 wt%, which does not seem to be abnormally high. However, this phosphorus level is already sufficient to facilitate intergranular SCC in a conventional 316 austenitic stainless steel if grain-boundary segregation exists [44]. A sulphur content of 0.08 wt% is quite high. Some researchers have stated that for applications demanding good ductility and toughness, the sulphur content mustn't exceed 0.020% [27]. While manganese tied up some of the sulphur to form manganese sulphides, it is certain that some sulphur would remain free in the present steel. In studying the hot cracking phenomenon of the simulated heat-affected zone of a type 308 austenitic stainless steel, Li and Messler [45] found sulphur to be more capable of segregating to grain boundaries than phosphorus. Additionally, Briant and Andresen [46] found sulphur to be more harmful than phosphorus in causing SCC in 0.005 M sulphuric acid (pH 2.5) at 288 °C. Consequently, it is believed that the high sulphur content of the present steel did play an important role in its intergranular fracture. As a matter of fact, very high contents of carbon and sulphur (especially the latter) of the economical chromium-manganese stainless steels have been flagged by researchers [13].

It must be noted that for solution-treated austenitic stainless steels, the fracture mode associated with Cl-SCC is usually (or predominantly) transgranular. Nevertheless, intergranular cracking of a non-sensitised, precipitate-free 316L austenitic-stainless-steel bellow was observed by Panda et al [43]. According to these authors, the martensite in the 316L steel bellow facilitated the transport of hydrogen (generated by the electrochemical reactions of the SCC process) to the grain boundaries, thereby expediting hydrogen embrittlement. The views by Panda and co-workers are in line with the hydrogen-embrittlement mechanism of solution-annealed austenitic stainless steels proposed by Nishimura and Alyousif [47]. In this mechanism, more efficient transport of hydrogen brought about by alpha-prime martensite, the hydrogen-enhanced localised plasticity at grain boundaries (which causes grain-boundary sliding), and the interactions between the alpha-prime martensite and grain-boundary-sliding-induced dislocation pileups all facilitate intergranular fracture.

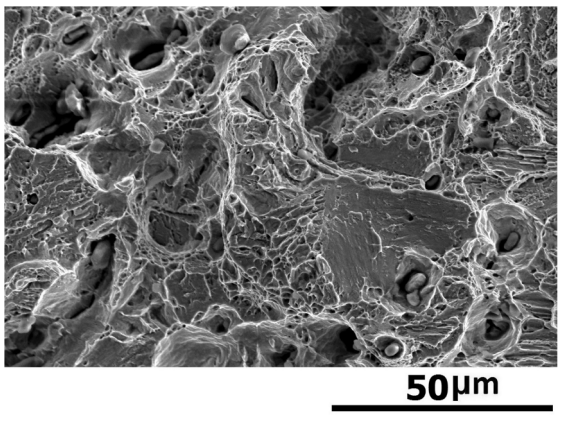

Fig. 13. High-magnification view of transgranular cracking of a sample pulled to failure in air at a strain rate of 10^{-1} s^{-1}.

However, for the present steel SSRTed in 60 °C NaCl, the influences of grain-boundary segregation of phosphorus and sulphur, and those of grain-boundary martensite seemed to be eclipsed by other factors. As shown above, the fracture mode was predominantly transgranular, with only sporadic pockets of intergranular cracking on the fracture surface (e.g., see the upper right corner of Fig. 11 (b). In fact, it may be seen in Fig. 5(a) that no grain boundaries had been revealed after polarisation test in 3.5% NaCl.

Wenman et al [48] proposed a transgranular Cl-SCC mechanism of austenitic stainless steels that involves the initiation of surface pits and the subsequent crack growth from the pit base under mechanical control. From Fig. 10 (d), it may be seen that the surface cracks tended to form within the grains and then grew transgranularly. The pit initiation sites were in-grain martensite (which is more anodic than austenite in a near neutral or in an acidic chloride-containing aqueous environment [49,50]), in-grain manganese sulphides [48] and possibly in-grain slip steps [51]. For a cold formed AISI 304 and a solution-treated 304L austenitic stainless steel, in-grain deformation-induced martensite was thought to contribute to its transgranular Cl-SCC [52,53]. It therefore appears that the in-grain pre-existing martensites and those formed during the crack growth process aided the transgranular fracture of the present steel. In-grain manganese sulphides of course also played a role.

4.2. Comments on the competing causes of fracture

As discussed above, when the present steel was SSRTed in air (strain rate: 10^{-6} s^{-1}), its fracture mode was predominantly intergranular. However, when it was pulled to fracture in air at the much higher strain rate of 10^{-1} s^{-1}, dimples could be seen on the fracture surface (Fig. 6 and Fig. 11(c)). When the fracture surface is examined at a high magnification (Fig. 13), it may be seen that some sporadic areas exhibiting cleavage also existed.

Interestingly, in the study of the SCC behaviour of some nitrogen-containing Fe18Cr10Mn-based austenitic stainless steels, Yoon et al [31] also noticed such a loss of intergranular feature on the fracture surfaces of their steels when the strain rate went up from 10^{-6} s^{-1} to 10^{-3} s^{-1}. They stated that further work was required to pinpoint the cause of change of fracture surface morphology. The present authors are also unclear about what caused this change of fracture mode.

For the present steel, Fig. 11 does show that when the strain rate was low, its fracture in air was mainly controlled by grain boundaries, which could be due to the segregation of phosphorus and sulphur. When the strain rate went up to sufficiently high values (e.g., 10^{-1} s^{-1}), nucleation of voids at inclusions (manganese sulphides in this case) and their growth and coalescence became the controlling factor of fracture. It therefore appears that when the strain rate was low, the strains at the inclusion/matrix interfaces could be better accommodated by the plasticity of the matrix during the deformation process. Hence, the fracture would be more governed by grain-boundary weakening associated with impurity elements.

5. Concluding remarks

Chromium-manganese stainless steels are meant to be substitutes for the more expensive 200 and 300 series austenitic stainless steels for less demanding applications. There have been reports of counterfeits being purposefully labelled as the 200 series or even the 300 series austenitic stainless steels. On the other hand, there are sellers who frankly acknowledge their products to be nonstandard, less-alloyed steels. However, even for the latter types of steels (not counterfeits), they are still well-known to contain high levels of carbon and impurities such as phosphorus and sulphur, as they are often produced by small steelmaking mills.

For the low-nickel, chromium-manganese ‘borderline’ stainless steel used for this paper, its strength and ductility are not too bad in air, despite its high levels of phosphorus and sulphur.

At the lower-bound temperature of chloride stress corrosion cracking of austenitic stainless steels (i.e., 60 °C), this steel shows some decrease of strength in 3.5% NaCl, but its ductility is not much reduced. The SSRT behaviour of this steel also deteriorates in 60 °C distilled water, and is not significantly different from that in NaCl. Consequently, cautions must be exercised even if this steel (and possibly similar steels as those reported in Refs. [3;14]) is used in a relatively benign environment.

The fracture modes of this steel SSRTed in air and in 60 °C distilled water are alike, i.e., predominantly intergranular without much necking. One of the reasons behind this is thought to be the high contents of phosphorus and sulphur (especially the latter).

The fracture mode of the present steel changes from being predominantly intergranular to being transgranular and dimpled when the strain rate increases (from 10^{-6} s^{-1} to 10^{-1} s^{-1}). This change of fracture mode with strain rate was also discovered in a FeCrMnNiNC high-interstitial austenitic stainless steel. The reason behind this strain-rate-dependent fracture mode change, however, is unclear.

The main point of this paper is that even if nonstandard, chromium-manganese stainless steels are sourced from unscrupulous sellers, the users should still heed that these steels may have high impurity levels (sulphur is particularly problematic). Segregation of impurities (sulphur in the present case) may cause intergranular SCC, while transgranular SCC may start from corrosion pits associated with manganese sulphides and in-grain martensite. Cautions should be exercised even if these steels are used in seemingly benign environments.

Declaration of Competing Interest

The authors declare that they have no known competing financial interests or personal relationships that could have appeared to influence the work reported in this paper.

Acknowledgements

This work reported was funded by The Science and Technology Development Fund, Macau SAR (057/2015/A2). The corrosion experiments were funded by the University of Macau through a Multi-Year Research Grant (MYRG2018-00030-FST).

References

[1] F. Moebus, J.M. Pardal, C.A. dos Santos, S.S.M. Tavares, P.A. Louzada, C. Barbosa, D.S. dos Santos, Eng. Fail. Anal. 74 (2017) 150.
[2] H. Binici, Eng. Fail. Anal. 14 (2007) 233.
[3] C. Qin, S. He, L. Zhong, W. Feng, J. Pang, Q. Li, W. He, Eng. Fail. Anal. 117 (2020), 104959.
[4] J.J. Fuentes, H.J. Aguilar, J.A. Rodriguez, E.J. Herrera, Eng. Fail. Anal. 16 (2009) 648.
[5] A. Vazdirvanidis, M. Bouzouni, G. Pantazopoulos, Eng. Fail. Anal. 110 (2020), 104432.
[6] G. Sussex, Aus. Stainless. Mag. 53 (2013) 4.
[7] M. Szala, K. Beer-Lech, M. Walczak, Eng. Fail. Anal. 77 (2017) 31.
[8] S.S.M. Tavares, J.M. Pardal, B.B. Almeida, M.T. Mendes, J.L.F. Freire, A.C. Vidal, Eng. Fail. Anal. 84 (2018) 1.
[9] X. Yang, M. Liu, Z. Liu, C. Du, X. Li, Eng. Fail. Anal. 116 (2020), 104729.
[10] K. Yang, Y. Ren, Sci. Technol. Adv. Mater. 11 (2010), 014105.
[11] International Stainless Steel Forum, "New 200-series" steels: An opportunity or a threat to the image of stainless steel?. Belgium. 2005.
[12] The European Stainless Steel Development Association (Euro Inox), Austenitic chromium-manganese stainless steels – a European approach. Materials and Applications Series. Vol. 12, 2012.
[13] J. Charlies, J. D. Mithieux, J. Krautschick, J. Antonio Simon, B. Van Hecke, T. Pauly, Revue Metall. 106 (2009) 90.
[14] W. Meng, S. Xu, M. Liu, Y. Zhao, Y. Zhang, Eng. Fail. Anal. 96 (2019) 44.
[15] Press Release No. 9/2018. European Anti-Fraud Office (https://ec.europa.eu/anti-fraud/media-corner/news/12-07-2018/major-seizure-counterfeit-steel-pipes-united-arab-emirates-following_en).
[16] D. S. Bae, M. H. Hong, Kazuya Miyahara, Solid. State. Commun. 125 (2003) 347.
[17] J.C. Lippold, D.J. Kotecki, Welding Metallurgy and Weldability of Stainless Steels, John Wiley and Sons, 2005.
[18] R. Rana, Mater. Sci. Technol. 35 (2019) 2039.
[19] J. Magee, Development of type 204 Cu stainless, a low-cost alternate to type 304. Carpenter Technology (https://www.carpentertechnology.com/blog/development-of-type-204-cu-stainless).
[20] A. Pardo, M.C. Merino, M. Carboneras, F. Viejo, R. Arrabal, J. Munoz, Corr. Sci. 48 (2006) 1075.
[21] D.N. Wasnik, Eng. Fail. Anal. 23 (2012) 69.
[22] H.Y. Ha, W.G. Seo, J.Y. Park, T.H. Lee, S. Kim, Mater. Charact. 119 (2016) 200.
[23] W.A. Spitzig, R.J. Sober, Metall. Trans. A. 8 (1977) 651.
[24] W.M. Guo, Z.C. Wang, Y.D. Li, J.B. Shi, Metall. Microstruct. Anal. 2 (2013) 249.
[25] S. Lynch, Eng. Fail. Anal. 100 (2019) 329.
[26] G. Barkleit, A. John, F. Schneider, Mater. Corr. 50 (1999) 591.
[27] C. Barbosa, J. L. do Nascimento, J. L. Fernandes, I. de Cerqueira Abud, J. Fail. Anal. Prevent. 8 (2008) 320.
[28] R.L. Klueh, P.J. Maziasz, E.H. Lee, Mater. Sci. Eng. A. 102 (1988) 115.
[29] J. Wan, Q. Ran, J. Li, Y. Xu, X. Xiao, H. Yu, L. Jiang, Mater. Des. 53 (2014) 43.
[30] S. Lee, C.Y. Lee, Y.K. Lee, J. Alloy. Compd. 628 (2015) 446.
[31] Y.S. Yoon, H.Y. Ha, T.H. Lee, S. Kim, Corr. Sci. 80 (2014) 28.
[32] N. Soloman, I. Solomon, Eng. Fail. Anal. 79 (2017) 865.
[33] A.I. Aljoboury, A.H.I. Mourad, A. Alawar, M.A. Zour, O.A. Abuzeid, Eng. Fail. Anal. 17 (2010) 1337.
[34] M.S. Kumar, M. Sujata, M.A. Venkataswamy, S.K. Bhaumik, Eng. Fail. Anal. 15 (2008) 497.
[35] M. Hamzeh, M.M. Karkehabadi, R. Jalali, Eng. Fail. Anal. 79 (2017) 431.
[36] W.B. Kan, H.L. Pan, Eng. Fail. Anal. 18 (2011) 110.
[37] M. Ghasri-Khouzani, J.R. McDermid, J. Mater. Eng. Perform. 28 (2019) 1591.
[38] X. Li, L. Chen, Y. Zhao, R.D.K. Misra, Mater. Des. 142 (2018) 190.
[39] J. Amini, A. Davoodi, H. Jafaria, Eng. Fail. Anal. 90 (2018) 440.
[40] M. Wang, L. Chen, X. Liu, X. Ma, Corro. Sci. 81 (2014) 117–124.
[41] K. Chandra, A. Mahanti, V. Kain, B.S. Kumar, N. Kumar, V. Gautam, Eng. Fail. Anal. 79 (2017) 642.
[42] D. Havel, Austenitic Manganese Steel – A Complete Overview. Columbia Steel Casting Co., Inc. 2017.
[43] B. Panda, M. Sujata, M. Madan, S.K. Bhaumik, Eng. Fail. Anal. 36 (2014) 379.
[44] P. McIntyre, C.M. Younes, S.W. Chan, Br. Corro. J. 31 (1996) 133.
[45] L. Li, R.W. Messler Jr, Weld. J. 81 (2002) 78s.
[46] C.L. Briant, P.L. Andresen, Metall. Trans. A. 19 (1988) 495.
[47] R. Nishimura, O.M. Alyousif, Corro. Sci. 51 (2009) 1894.
[48] M.R. Wenman, K.R. Trethewey, S.E. Jarman, P.R. Chard-Tuckey, Acta. Mater. 56 (2008) 4125.
[49] Z. Zhang, G. Pan, Y. Jiang, S. Chen, S. Zou, W. Li, C. Xu, J. Zhang, Materials. 12 (2019) 4025.
[50] A. Chiba, I. Muto, Y. Sugawara, N. Hara, Mater. Trans. 55 (2014) 857.
[51] A. Poonguzhali, S. Ningshen, G. Amarendra, Metal Mater. Intl. 26 (2020) 1545.
[52] I. Park, E.Y. Kim, W.J. Yang, Metals. 11 (2021) 7.
[53] S.S. Birley, D. Tromans, Corrosion. 27 (1971) 63.